NASA Technical Memorandum 102426
AIAA-90-0339

Unsteady Euler Analysis of the Flow Field of a Propfan at an Angle of Attack

M. Nallasamy
Sverdrup Technology, Inc.
NASA Lewis Research Center Group
Cleveland, Ohio

and

J.F. Groeneweg
National Aeronautics and Space Administration
Lewis Research Center
Cleveland, Ohio

Prepared for the
28th Aerospace Sciences Meeting
sponsored by the American Institute of Aeronautics and Astronautics
Reno, Nevada, January 8-11, 1990

NASA

UNSTEADY EULER ANALYSIS OF THE FLOWFIELD OF A PROPFAN AT AN ANGLE OF ATTACK

M. Nallasamy
Sverdrup Technology, Inc.
NASA Lewis Research Center Group
Cleveland, Ohio 44135

and

J.F. Groeneweg
National Aeronautics and Space Administration
Lewis Research Center
Cleveland, Ohio 44135

Abstract

The paper examines the effects of angle of attack of a propfan on the blade loading and details of the flowfield by solving the unsteady three-dimensional Euler equations. The configuration considered is the SR7L propeller at cruise condition and the inflow angles considered are 4.6°, 1.6° and -0.4°. The results indicate that the blade response is nearly sinusoidal at low inflow angles (1.6° and -0.4°) and significant deviations from sinusoidal behavior occur at an inflow angle of 4.6° due to the presence of strong shocks on both suction and pressure surfaces of the blade. The detailed flow in the blade passages shows that a shock formed on the suction surface during the highly loaded portion of the revolution extends across the passage to the pressure surface. An increase in inflow angle results in an increase in blade loading on the down-going side and a decrease in loading on the up-going side.

Introduction

The flowfield of an advanced propeller is complex due to the sweep, twist, and taper of the blade. Wind tunnel tests and flight tests have been conducted on a large scale 9-ft diameter advanced propeller (SR7L) to understand the aerodynamics and acoustics of the advanced design. Steady and unsteady blade pressure measurements were carried out on a two bladed configuration in wind tunnel tests.[1-3] A systematic investigation of the propfan characteristics was conducted in flight tests on an eight bladed (SR7L) configuration under the propeller test assessment (PTA) program.[4,5]

In the flight test program, a nacelle tilt arrangement was employed to vary the inflow angle to the propfan. The variations in inflow conditions were used to study the near-field noise characteristics of of the propfan. The nacelle tilt angles considered were -3°, -1° (tilt down) and 2° (tilt up). The average inflow angle to the propfan is dependent on the airplane angle of attack, upwash angle at the propfan and nacelle tilt. For the cruise operating conditions of interest here, the airplane angle of attack was 1.6°. The upwash angle at the propfan estimated from panel method calculations is 1.0°. Thus the estimated inflow angles[5] corresponding to the nacelle tilt angles -3°, -1°, and 2° are 4.6°, 1.6°, and -0.4°, respectively. Near-field acoustic data were acquired over a range of operating conditions. Of interest here is the effect of inflow angle on the measured sound pressure levels (SPL) at the outboard wing boom microphones and inboard fuselage microphones. Measurements showed that with an increase in inflow angle, SPL at the outboard wing boom increased while the SPL at the inboard fuselage decreased.[5,6] The rotation of the propfan was inboard-up.

Prediction of the effect of inflow angle on the near-field noise requires knowledge of the unsteady flowfield of the propfan. The solution of the unsteady three-dimensional Euler equations appears to be a promising approach. The three-dimensional Euler solution of the propfan at an angle of attack was first reported by Whitfield et al.[7] They found a fairly good agreement of the predicted unsteady blade pressures with the wind tunnel data for the SR3 model propeller. Nallasamy and Groeneweg[8] studied the effect of inflow angle on the blade loading for the SR7L eight bladed PTA configuration for an inflow angle of 4.6°. They presented detailed spanwise, chordwise and azimuthal pressure variations due to angle of attack. The results show a nearly sinusoidal response of the integrated blade loading and the first harmonic dominates the loading. The blade is lightly loaded for part of the revolution and shocks appear on both surfaces of the blade from hub to 90 percent radial station for the highly loaded portion of the revolution.

In the present paper, the effect of inflow angle is further studied by obtaining unsteady three-dimensional Euler solutions for 1.6° and -0.4° inflow angles (corresponding to the nacelle tilt angles of -1° and -3° of the PTA flight test program). The results obtained here are analyzed together with that obtained for an inflow angle of 4.6°[8] to understand the effect of inflow angle on the flowfield and blade loading. The azimuthal variation of the flow in the blade passage, chordwise loading and blade surface pressures are examined. The blade loading variation as a function of inflow angle is illustrated.

Numerical Solution of Unsteady Three-Dimensional Euler Equations

The unsteady three-dimensional Euler equations governing the inviscid flow through a propeller are solved employing a solution procedure developed by Whitfield et al.[7,9] A brief description of the solution procedure is given here. Further details may be found in the references cited. The Euler equations in conservative differential form are transformed from a Cartesian reference frame to a time dependent body fitted curvilinear reference frame. The transformed equations are discretized employing a finite volume technique. An approximate Riemann solver is used for block interface flux definitions. A Lower-Upper (LU) implicit numerical scheme is used to solve the discretized equations. The flowfield is represented by multi-

block composite grids to overcome computer core memory limitations. The solution at each time step is updated by having only one block in memory while other blocks are stored in solid-state storage devices (SSD). The same solution procedure was employed by the authors in Ref. 8.

Computational Grid

The configuration considered is the eight bladed SR7L propfan. The direction of rotation of the propfan and the axes of reference are shown in Fig. 1(a). An H-grid is employed to represent the flowfield. Each blade passage is described by 71 by 33 by 11 (axial by radial by circumferential) grid points. Each passage grid is divided into two blocks (71 by 33 by 6 each) for computational convenience as mentioned earlier. Thus, 16 blocks of grids are employed to describe the entire flowfield (eight passages) with 206,184 nodal points. Each blade surface is represented by 35 by 21 (chordwise by spanwise) grid points with higher resolution near the leading and trailing edges. The grid distribution employed here is the same as that used in Ref. 8. Figure 1(b) defines the azimuthal angle of the blades and blade passages at an instant of time for which blade surface pressures, blade loading and pressure distribution in the blade passages are presented and discussed in the next section.

Results and Discussion

The unsteady three-dimensional Euler solutions were obtained for two inflow angles, 1.6° and -0.4° at cruise conditions, Mach number is 0.801 and advance ratio is 3.122. These solutions are examined together with that obtained for an inflow angle of 4.6° in Ref. 8, at the same cruise conditions. The present solutions were obtained from an impulse start for three complete revolutions of the the propeller, to obtain a reasonably accurate solution. The results of the third revolution are stabilized as indicated by a nearly constant value of the computed total power coefficient of the propeller during the third revolution of the propeller. The results of the third revolution are analyzed and presented here. The predicted total power coefficients are nearly the same for all the three inflow angles and are about 8 percent higher than the measured value. Detailed chordwise pressure distributions are unavailable for this configuration for direct comparison. However, the present solution technique has been employed to predict the unsteady blade surface pressures on a two bladed SR7L propeller wind tunnel test configuration. The predicted chordwise pressure distribution has been found to agree reasonably well with the data.[10] The present blade surface grid distribution was also used to predict the steady blade surface pressure distributions and found to result in solutions which are in agreement with wind tunnel data.[11]

Figure 2 shows the variation of the single blade power coefficient with azimuth angle for three inflow angles: 4.6°, 1.6°, and -0.4°. The blade starts in each case at $\phi = 0°$ and the variation of the power coefficient of this blade is shown for three revolutions. The expected nearly sinusoidal variation of the blade loading due to angle of attack is clearly observed in all cases. The amplitude of the sinusoidal variation of course depends on the inflow angle and varies up to ±81 percent for $\alpha = 4.6°$, ±36 percent for $\alpha = 1.6°$ and ±6 percent for $\alpha = -0.4°$. The curve for $\alpha = 1.6°$ shows nearly the same trend as that for 4.6° inflow angle. The curve for $\alpha = -0.4°$ shows 180° phase shift from the other two cases; the maximum blade loading for this case occurs near an azimuth angle where minimum loading occurs for $\alpha = 1.6°$ and 4.6° or vice versa.

A Fourier transform of the third cycle variation of blade power coefficient gives cp as $cp = a_0 - a_i \cos wt - b_i \sin wt$. The loading spectra are shown in Fig. 3. The figure shows that the mean loading is the same for all the three inflow angles and first harmonic dominates the loading. However, the levels of the first harmonic are quite different; for $\alpha = 4.6°$ the level of the first harmonic is nearly equal to the mean value, while for $\alpha = 1.6°$ and -0.4° inflow angles first harmonic levels are much lower than the mean value. The angle by which the first harmonic loading lags the blade motion for the three cases, $\alpha = 4.6°$, 1.6° and -0.4°, are 14.4°, 16.3° and 8.5°, respectively.

The effect of inflow angle on the chordwise loading is described in Figs. 4 to 6. The figures show azimuthal variations of chordwise loading for three radial stations namely r/R = 0.47, 0.66 and 0.85. At each radial station and azimuthal position loading distribution for all the three inflow angles are shown. Figure 4 shows the azimuthal variation of chordwise loading at r/R = 0.47. One observes immediately that the the blade loading is a complex function of azimuthal position, inflow angle and chordwise location. Significant azimuthal variations in loading are observed for all inflow angles including $\alpha = -0.4°$. As shown in Fig. 2, the single blade loading for $\alpha = -0.4°$ is 180° out of phase as compared to the other two inflow angles. This shows up as higher chordwise loading for $\alpha = -0.4°$ than for $\alpha = 1.6°$ and 4.6°, at $\phi = 0°$, 45°, 90° and 315° azimuthal positions. The extent of negative loading that occurs for $\phi = 0°$ and 90° locations gradually reduces with reduction in inflow angle; for $\alpha = -0.4°$ no negative loading occurs at any azimuthal location for this radial station.

If one looks for trends in loading variation with inflow angle, no single trend is easily recognizable; for $\phi = 0°$ to 45° the blade loading decreases with increase in inflow angle for most part of the chord; for $\phi = 90°$ loading decrease with increase in α for 0 to 75 percent chord while for the rest of the chord length variations are small; for $\phi = 135°$ and 180° the loading increases with for most part of the chord except for the mid section; for $\phi = 225°$ and 270° the loading increases with increase in α for the entire chord length; and for $\phi = 315°$ the loading variations with α revert to the one similar to that at $\phi = 0°$.

The azimuthal variations of chordwise loading at r/R = 0.66 are shown in Fig. 5 for all three inflow angles. The loading variations at this spanwise station are more complex but similar to that observed at r/R = 0.47 for most part of the blade revolution and chord length. The exceptions are: (1) increase in the extent of the chord length in which no significant change in loading with α occurs at $\phi = 90°$; (2) a similar increase in the extent of no significant change

at $\phi = 270°$; and (3) at $\phi = 315°$ the loading variations near the leading edge region do not revert to that at $\phi = 0°$ as for the radial location $r/R = 0.47$.

Figure 6 presents the azimuthal variations of loading at $r/R = 0.85$ for all the inflow angles studied. The loading variations at this radial station are smooth compared to the other two radial stations ($r/R = 0.47$ and 0.66). Exceptions are the curves for $\alpha = 4.6°$ at $\phi = 135°$ and 180° locations; the shapes of the curves here are related to the shocks on the pressure side for this inflow angle. It is also seen that uniform loading occurs for most part of the revolution of the blade. However, for $\phi = 0°$ to 90° the loading decreases with increase in α and for $\phi = 180°$ to 270° it increases with α. The azimuthal locations $\phi = 135°$ and 315° are the transition locations where the above loading trends change from one to the other.

A Fourier transform of the azimuthal variation of the loading at any point on the blade gives the contributions of the harmonics at that location. Chordwise variations of the loading harmonics at the radial station $r/R = 0.66$ are shown in Fig. 7. The figure shows the real and imaginary parts of the loading for the first three harmonics at all the three inflow angles. It is seen that at $\alpha = 4.6°$, first three harmonics show significant chordwise variations. For low inflow angles ($\alpha = 1.6°$ and $-0.4°$) only the first harmonic shows significant chordwise variation.

The loading variations become somewhat easy to comprehend if we look at the actual blade surface pressures. We present the azimuthal variation of blade surface pressures only for the radial station $r/R = 0.66$ (Fig. 8). As discussed by the authors in Ref. 8, shocks appear on both suction and pressure surfaces during the highly loaded part of the revolution for $\alpha = 4.6°$. For an inflow angle of 1.6° a similar flow behavior is observed. The trailing edge shock on the suction surface from $\phi = 130°$ to 270°, has shock strength lower than that for $\alpha = 4.6°$. The shock extends to the pressure side for $\phi = 135°$ to 225°, and is also weaker than that for 4.6°. For an inflow angle of $-0.4°$ the picture is quite different because of the 180° phase difference in loading between this case and that of positive inflow angles; strong trailing edge shocks appear at $\phi = 0°$, 45°, 270° and 315° for $\alpha = -0.4°$, while at the remaining azimuthal position it is weaker than that of $\alpha = 1.6°$ to 4.6°. Only a relatively weak shock appears on the pressure side for azimuthal positions $\phi = 0°$, 45° and 315°.

Transonic flows over oscillating airfoils have been extensively studied and documented.[12] No such detailed experimental data are available for three-dimensional transonic flows of the propfan considered here. As discussed in Ref. 8 and also observed here for angles of attack 1.6 and -0.4, unsteady three-dimensional Euler solutions seem to indicate the presence of shock motions in three-dimensional transonic flows similar to those observed in two-dimensional transonic flows.

The detailed flowfield information in blade passages are presented in Figs. 9 to 11 in the form of static pressure contours at the spanwise station $r/R = 0.66$ for all the inflow angles. The static pressure contours in all eight blade passages for an inflow of 4.6° are shown in Fig. 9. In a steady flow ($\alpha = 0$), all the eight passage contours will be identical. But for an angle attack of 4.6° significant flow changes occur in the blade passages. No shock formation is observed in the lightly loaded part of the revolution. The strong shock formed in the trailing edge region of suction surface in the highly loaded part of the revolution extends across the passage to the pressure side of successive blade. The axial location at which the shock appears on pressure surface depends on the azimuth angle. The passage denoted by $\phi = 135°$ to 180° is the one in which the shock location on the pressure side is closest to the trailing edge and the shock has highest strength. It should be noted that the pressure variations in Fig. 8 refer to the suction and pressure side of the same blade whereas Figs. 9 to 11 refer to suction side of one blade and pressure side of the successive blade.

Figure 10 shows the static pressure contours in the blade passages at $r/R = 0.66$ for an inflow angle of 1.6°. As noted earlier, the flow characteristics for this inflow angle are similar to that of 4.6° inflow. It is observed that the shocks on the pressure surface are of lower strength and appear farther from the trailing edge for the passages $\phi = 135°$ to 180° and $\phi = 180°$ to 225°, when compared with the corresponding ones of $\alpha = 4.6°$.

The pressure contours in the blade passages for an inflow angle of $-0.4°$ are shown in Fig. 11. In this case the flow details are quite different from that for $\alpha = 1.6°$ or 4.6°. A trailing edge shock whose strength depends on the azimuthal angle appears on the suction surface. In most passages, the shock diffuses before it reaches pressure surface. Weak shocks seem to reach pressure surface in the passages marked $\phi = 0°$ to 45°, 45° to 90° and 315° to 0°.

The azimuthal variations of elemental power coefficient, dcp/dx ($x = r/R$) are shown in Fig. 12. Figure 12(a) shows the elemental power coefficient variation for an inflow angle of 4.6° at four azimuthal locations, $\phi = 0°$, 90°, 180° and 270°. Also shown in the figure is the curve for the steady flow ($\alpha = 0°$). The shape of the curve for any azimuthal position is similar to that of steady flow. The magnitude of the cyclic variation of loading depends on the spanwise location. The elemental power coefficient variation for an inflow angle of 1.6° is shown in Fig. 12(b). The trends of the curves with azimuthal angle are similar to that of 4.6°; higher loading levels occur for $\phi = 180°$ and 270° positions and lower loading levels occur at $\phi = 0°$ and 90° locations. But the magnitudes of loading at any radial station are much smaller. Figure 12(c) shows the elemental power coefficient variation for $\alpha = -0.4°$. The cyclic loading variations are 180° out of phase compared to the positive inflow angles (1.6° and 4.6°); higher loading levels occur at $\phi = 0°$ and 90° and lower loading levels occur at $\phi = 180°$ and 270°. Also, the magnitude of cyclic variation as compared to the steady flow is very small (consistent with Fig. 2).

The rotation of the propfan is inboard-up (Fig. 1); i.e., the blade is going up at $\phi = 0°$ (fuslage side) and down at $\phi = 180°$ (on the outboard side). The blade is expected to be highly

loaded when it goes down and lightly loaded when it goes up, for positive inflow angles. The variations of elemental power coefficient with inflow angle are shown in Fig. 13, for four azimuthal locations: ϕ = 0°, 90°, 180° and 270°. At ϕ = 0°, (Fig. 13(a)) the loading decreases with an increase in inflow angle. Thus, at this azimuthal location the highest loading levels occur for an inflow angle of -0.4°. At the azimuthal location ϕ =180° (Fig.13(c)) the blade loading increases with increase of angle of attack, resulting in the highest loading levels for α = 4.6°. The loading variations at ϕ = 90° (Ref. 13(b)) are similar to that at ϕ = 0° (loading decreases with increase of inflow angle). At ϕ = 270° (Fig.13(d)) the loading variation is similar to that at ϕ = 180° (loading increases with increase in inflow angle).

Comparisons of blade responses with angle of attack are presented for two axial locations (x/c = 0.125 and 0.63) in Fig. 14, for a spanwise station r/R = 0.66. The figure shows the variations of pressure coefficient during one revolution of the blade for all the three inflow angles considered. The amplitude of the wave increases with an increase of the inflow angle. For low inflow angles (α = 1.6° and -0.4°) the response is nearly sinusoidal at both axial locations and also on both suction and pressure surfaces. The response at α = 4.6° is nearly sinusoidal only on the suction surface at x/c = 0.125 (Fig. 14(a)). Large deviations from sinusoidal response occur at all other points shown (Fig. 14(b) to (d)). These deviations are due to the appearance of strong shocks for this inflow angle as observed in Fig. 8. Thus, the blade response becomes complicated for high inflow angles. The response also depends on the axial location on the blade and the surface (suction or pressure surface) on which the point is located.

Concluding Remarks

The effect of angle of attack of propfan to the mean flow was studied by solving the three-dimensional Euler equations. Three inflow angles, 4.6°, 1.6° and -0.4° were considered. The results of the positive inflow angles (4.6° and 1.6°) show similar trends. The negative inflow angle produces an integrated blade loading which is 180° out of phase when compared to that of positive angles. For the inflow angles 4.6 and 1.6 strong shocks appear on both surfaces of the blade during the highly loaded part of the revolution. At -0.4° inflow angle the blade loading variations during the revolution are small. The detailed flow in the blade passages clearly indicate to the strong shocks extending from suction to pressure surface during the highly loaded part of the revolution. An expected, an increase in angle of attack increases the loading on the down-going (outboard) side, while loading on the up-going (fuselage) side decreases, for the range of inflow angles considered here.

Acknowledgements

The results reported here were obtained using the computer code developed by Prof. Whitfield. Part of the computations were done on NAS Computer system. The authors wish to acknowledge the graphics support of Jeff Hanson and Susan Adato.

References

1. Bushnell, F., "Measurement of the Steady Surface Pressure Distribution on a Single Rotation Large Scale Advanced Propfan Blade at Mach Numbers from 0.03 to 0.78," NASA CR-182124, 1988.

2. Bushnell, P., Gruber, M., and Parzych, D., "Measurement Of Unsteady Blade Surface Pressures on a Single Rotation Large Scale Advanced Propfan with Angular and Wake Inflow at Mach Numbers from 0.02 to 0.70," NASA CR-182123, 1988.

3. Campbell, W.A., Wainauski, H.S., and Bushnell, P.R., "A Report on High Speed Wind Tunnel Tests of the Large Scale Advanced Propfan," AIAA Paper 88-2802, July 1988.

4. Poland, D.I., Bartel, H.W., and Brown, P.C., "PTA Flight Test Overview--Propfan Test Assessment," AIAA Paper 88-2803, July 1988.

5. Little, B.H., Bartel, H.H., Reddy, N.N., Swift, G., and Withers, C.C., "Propfan Test Assessment (PTA) Flight Test Report," NASA-CR-182278, 1989.

6. Bartel, H.W., and Swift, G., "Near-Field Acoustic Characteristics of a Single-Rotor Propfan," AIAA Paper 89-1055, April 1989.

7. Whitfield, D.L., Swafford, I.W., Janus, J.M., Mulac, R.A., and Belk, D.M., "Three Dimensional Unsteady Euler Solutions for Propfans and Counter-Rotating Propfans," AIAA Paper 87-1197, June 1987.

8. Nallasamy, M., and Groeneweg, J.F., "Prediction of Unsteady Blade Surface Pressures on an Advanced Propeller at an Angle of Attack," AIAA Paper 89-1060, Apr. 1989.

9. Janus, J.M., and Whitfield, D.L., "A Simple Time Accurate Turbomachinery Algorithm with Numerical Solutions Of Uneven Blade Count Configuration," AIAA Paper 89-0206, Jan. 1989.

10. Nallasamy, M., amd Groeneweg,, J.F., "Unsteady Blade Surface Pressures on a Large Scale Advanced Propeller: Prediction and Data," to be presented at the Joint Propulsion Conference, 1990.

11. Nallasamy, M., Yamamoto, O., Warsi, S., and Bober, L.J., "Large Scale Advanced Propeller Blade Pressure Distributions: Prediction and Data," AIAA Paper 89-2696, July 1989.

12. Tijdeman, H., and Seebass. R., "Transonic Flow Past Oscillating Airfoils," Annual Review of Fluid Mechanics, Vol. 12, 1980, pp. 181-222.

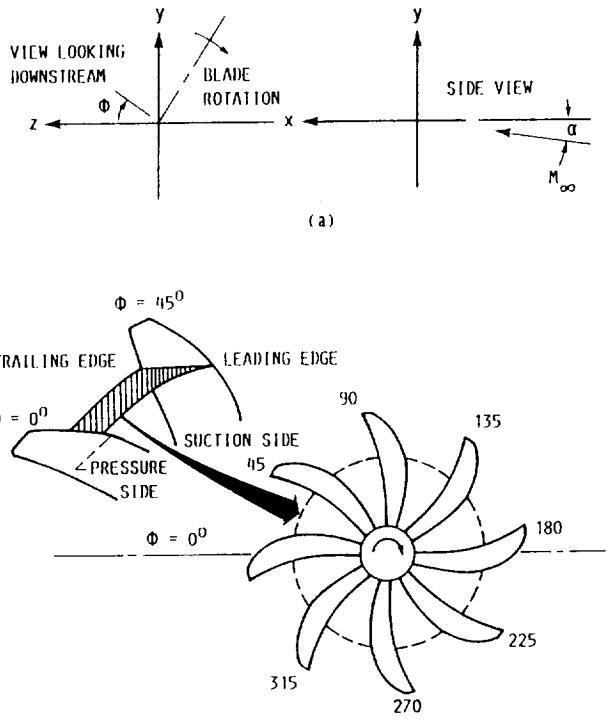

FIGURE 1. - AXES OF REFERENCE AND DEFINITION SKETCH.

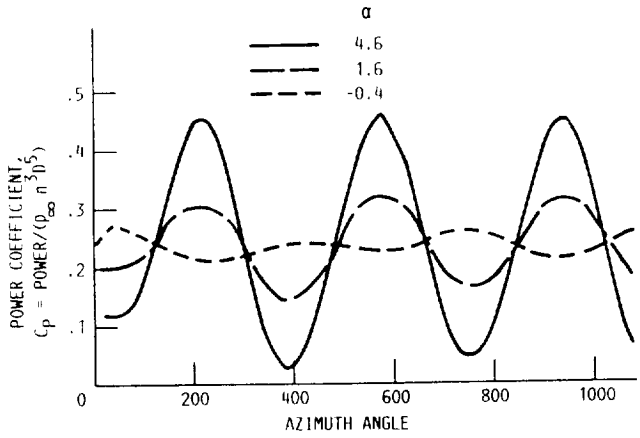

FIGURE 2. - POWER PER BLADE VARIATION WITH AZIMUTH ANGLE.

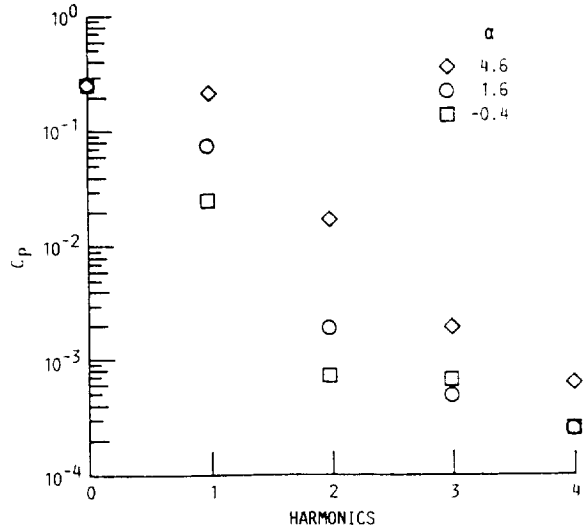

FIGURE 3. - LOADING SPECTRUM.

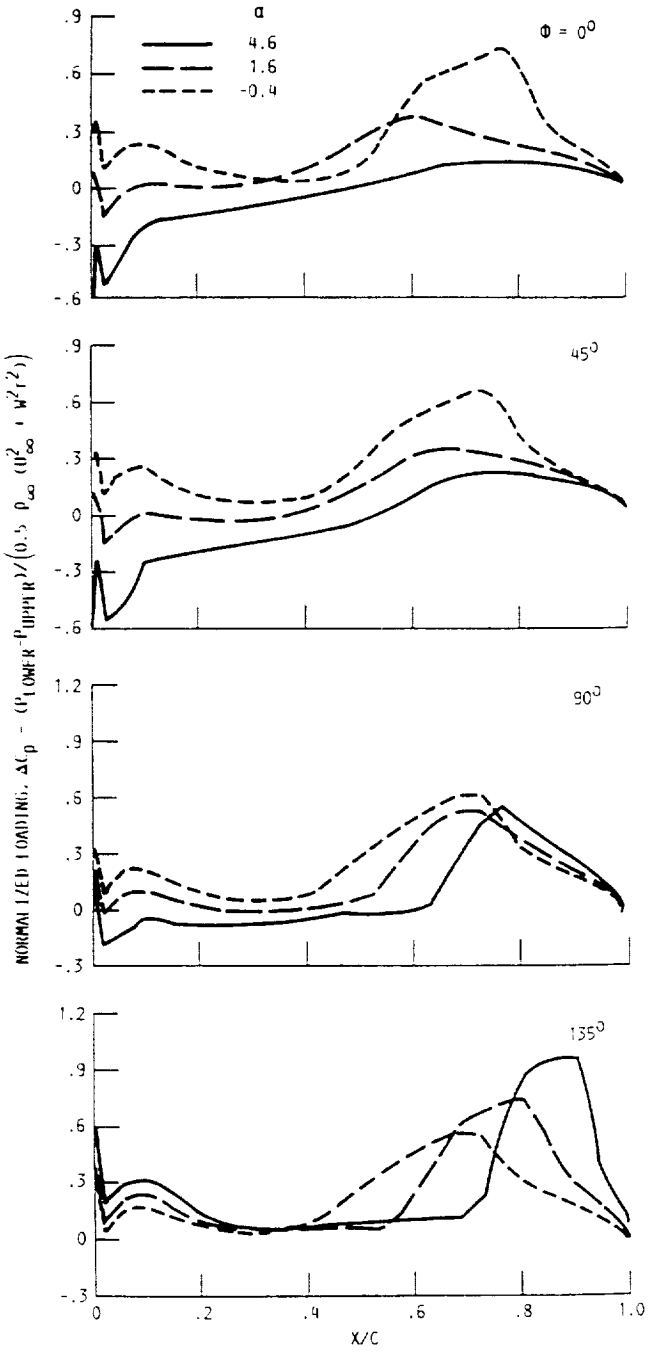

FIGURE 4. - AZIMUTHAL VARIATION OF CHORDWISE LOADING AT r/R = 0.47.

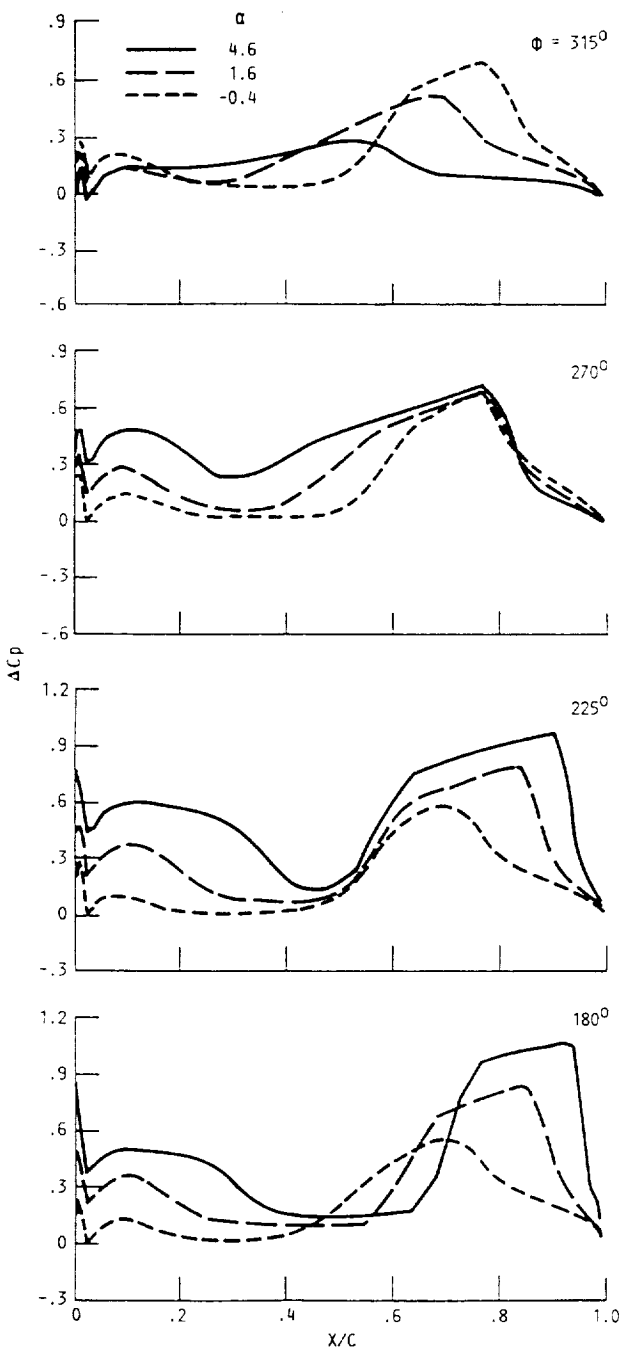

FIGURE 4. - CONCLUDED.

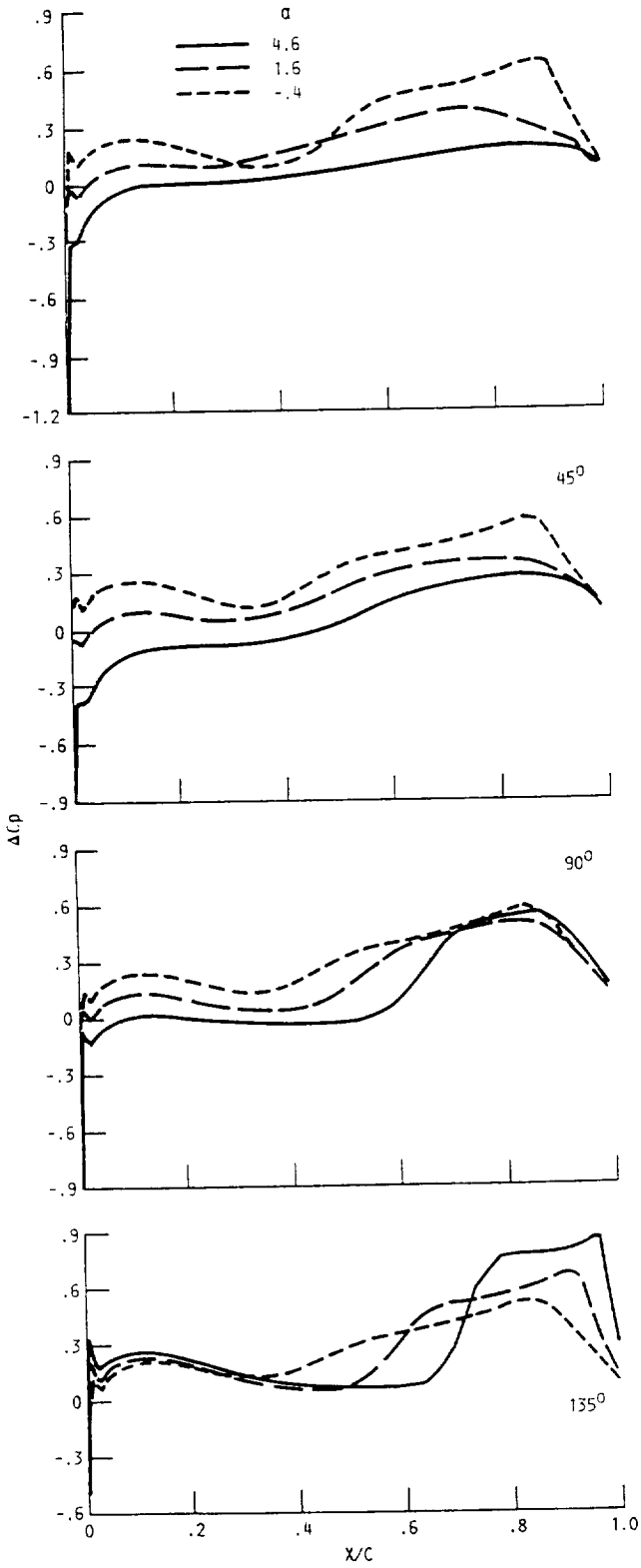

FIGURE 5. - AZIMUTHAL VARIATION OF CHORDWISE LOADING AT r/R = 0.66.

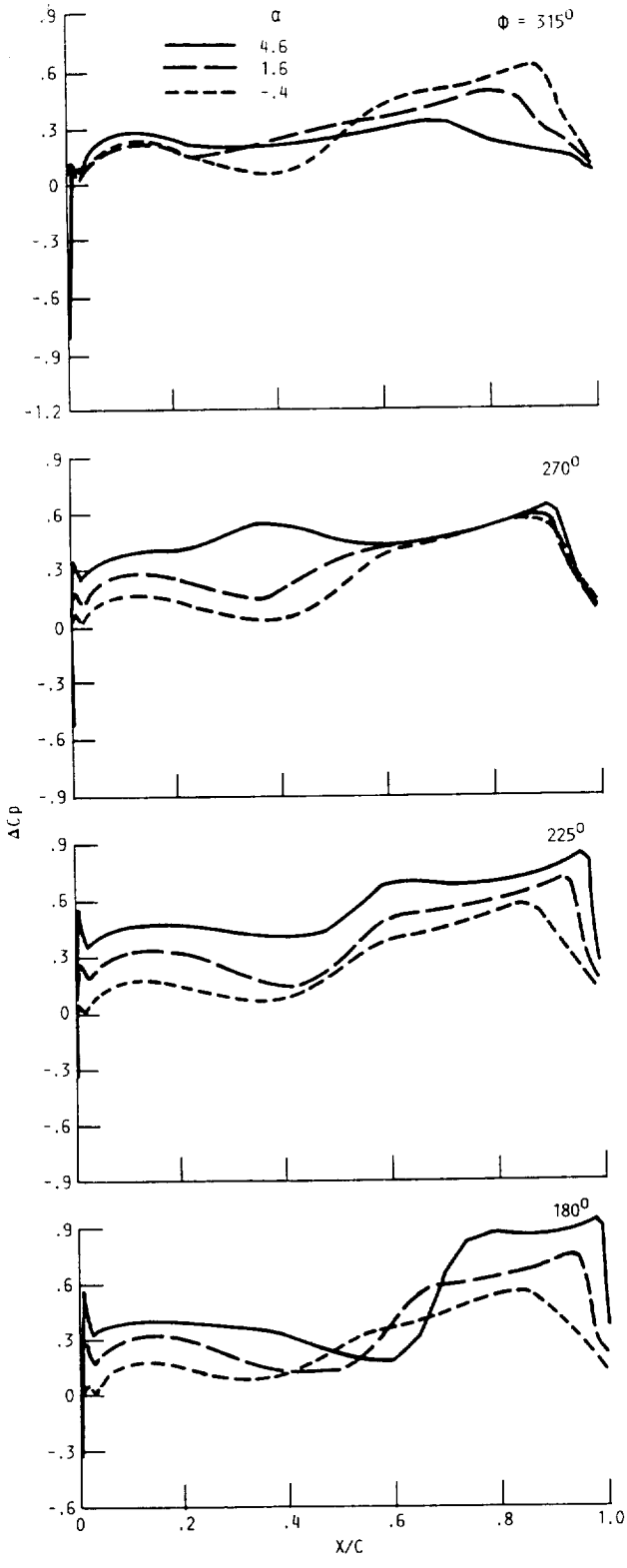

FIGURE 5. - CONCLUDED.

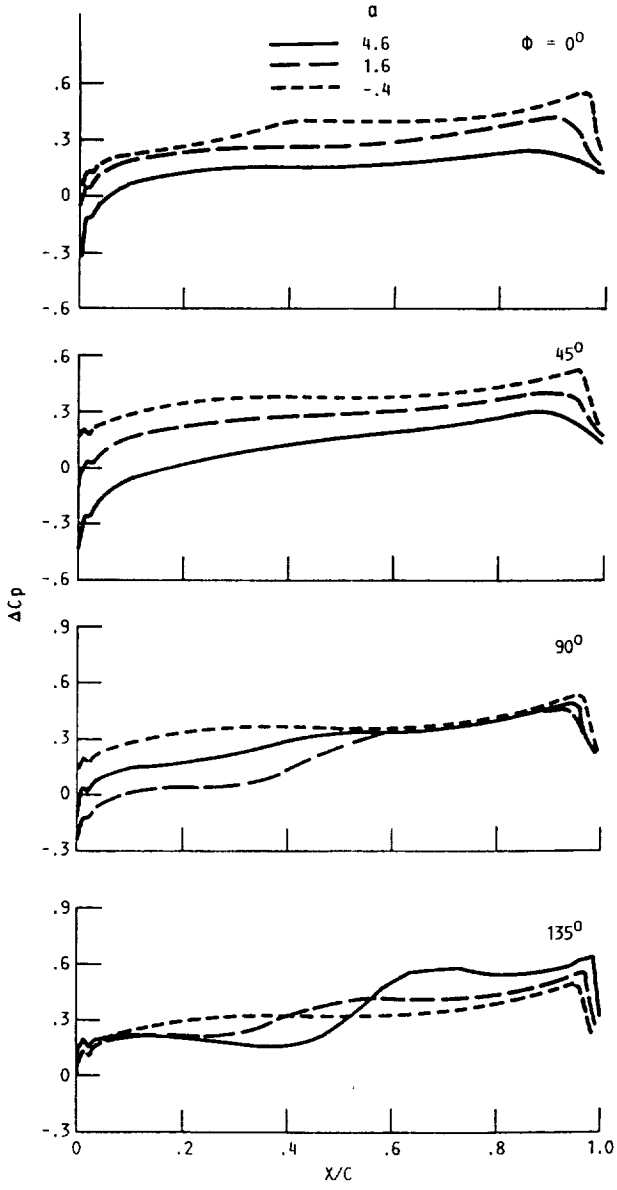

FIGURE 6. - AZIMUTHAL VARIATION OF CHORDWISE LOADING AT r/R = 0.85.

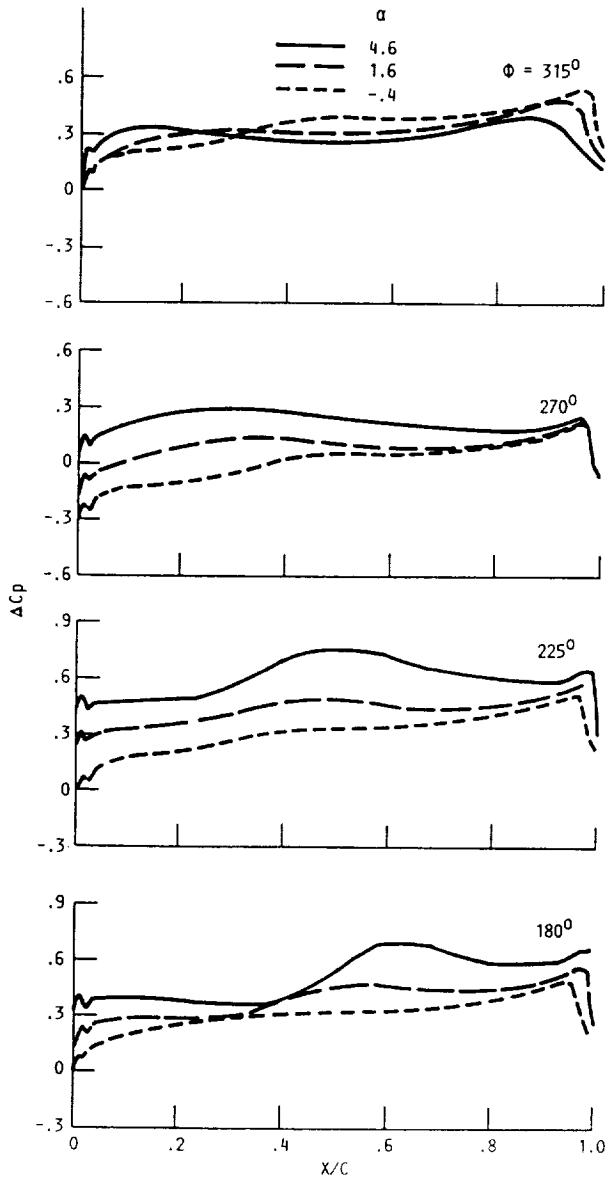

FIGURE 6. - CONCLUDED.

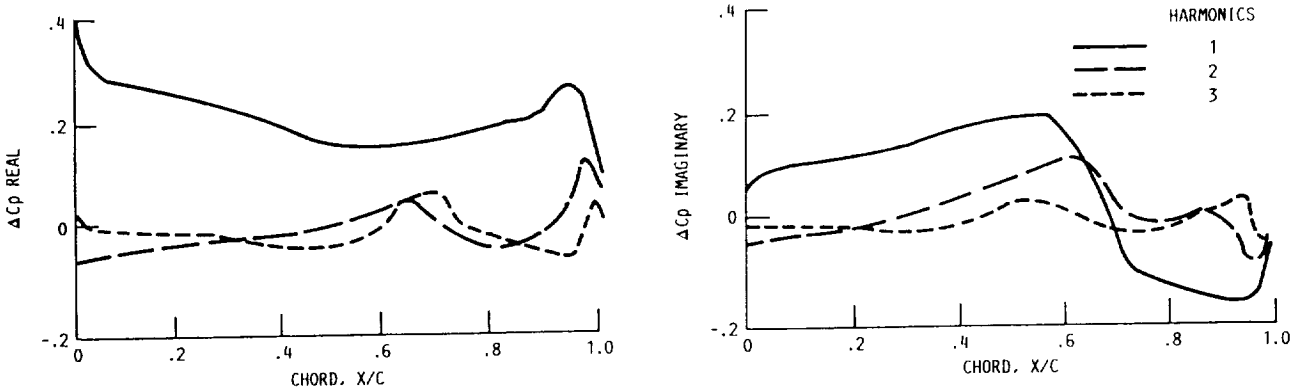

(a) α = 4.6.

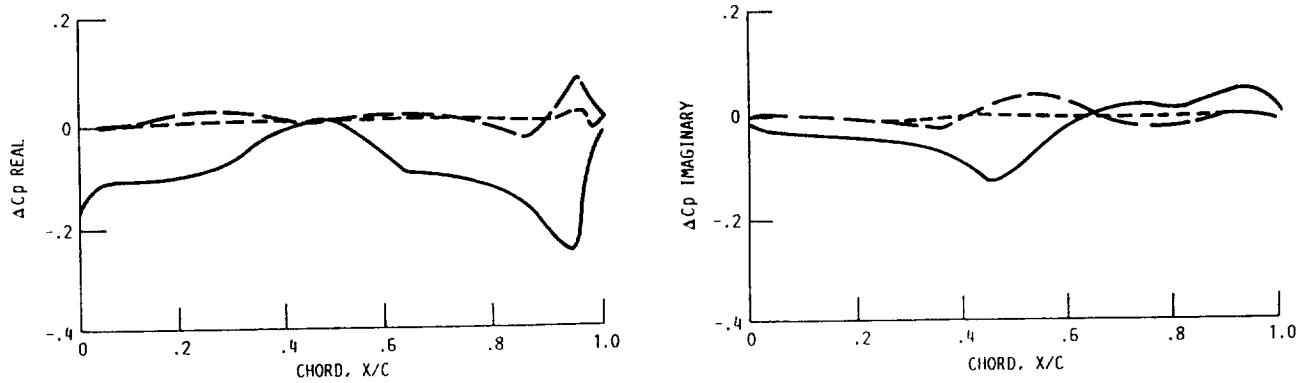

(b) α = 1.6.

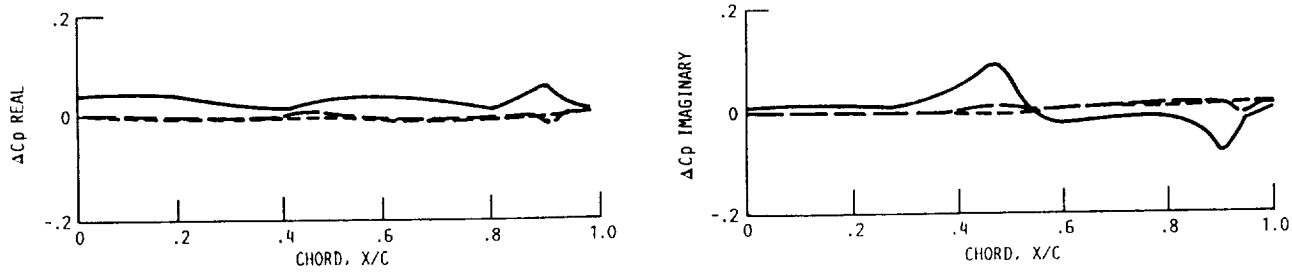

(c) α = -0.4.

FIGURE 7. - LOADING HARMONICS AT r/R = 0.66.

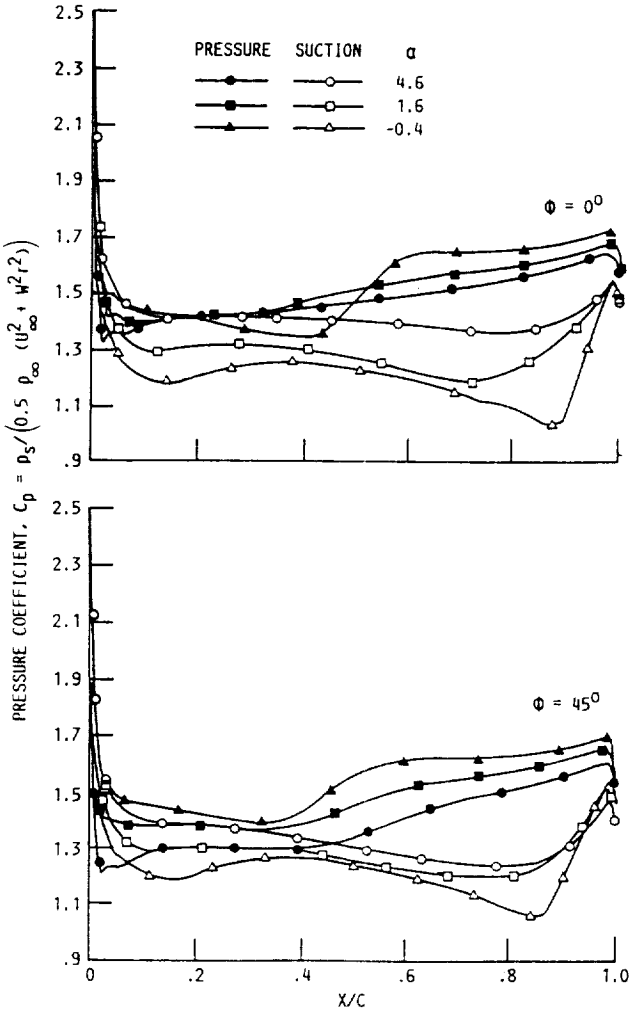

FIGURE 8. - AZIMUTHAL VARIATION OF BLADE SURFACE PRESSURES AT r/R = 0.66.

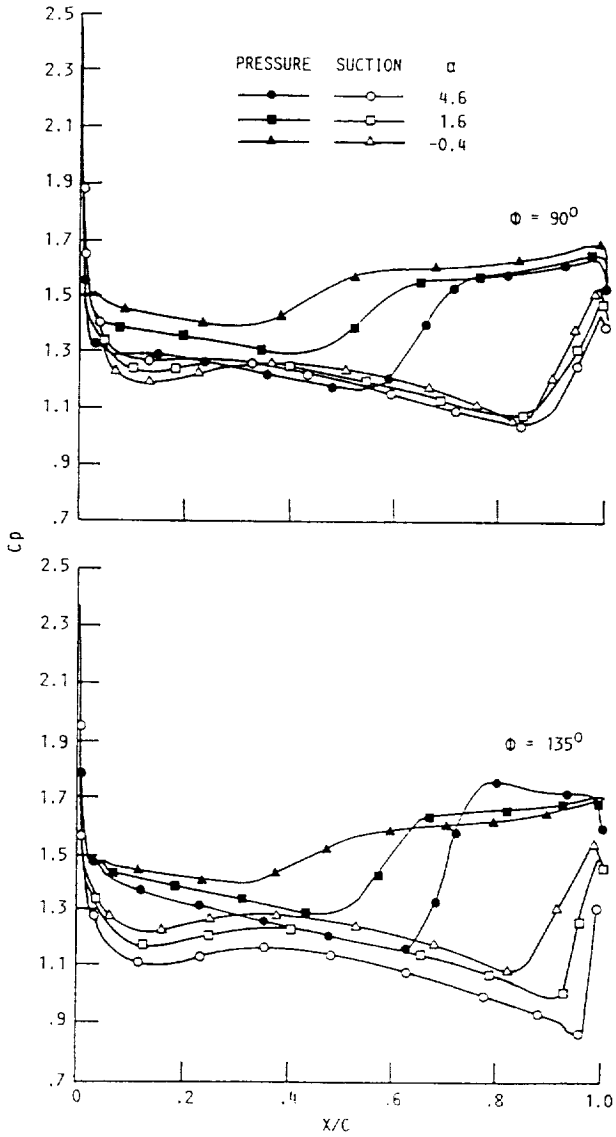

FIGURE 8. - CONTINUED.

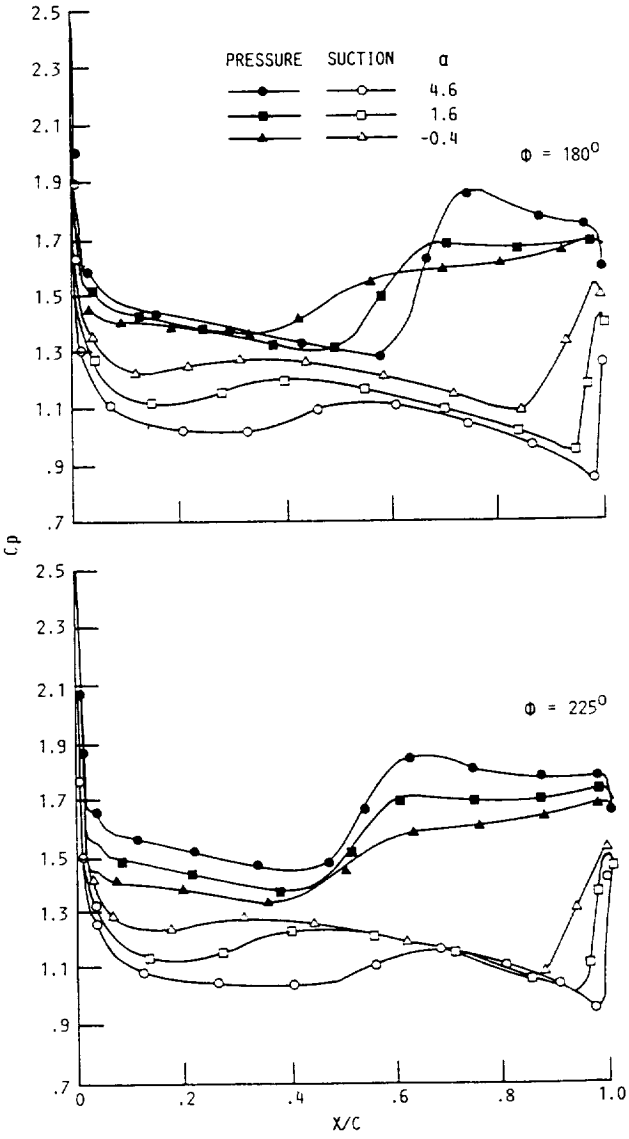

FIGURE 8. - CONTINUED.

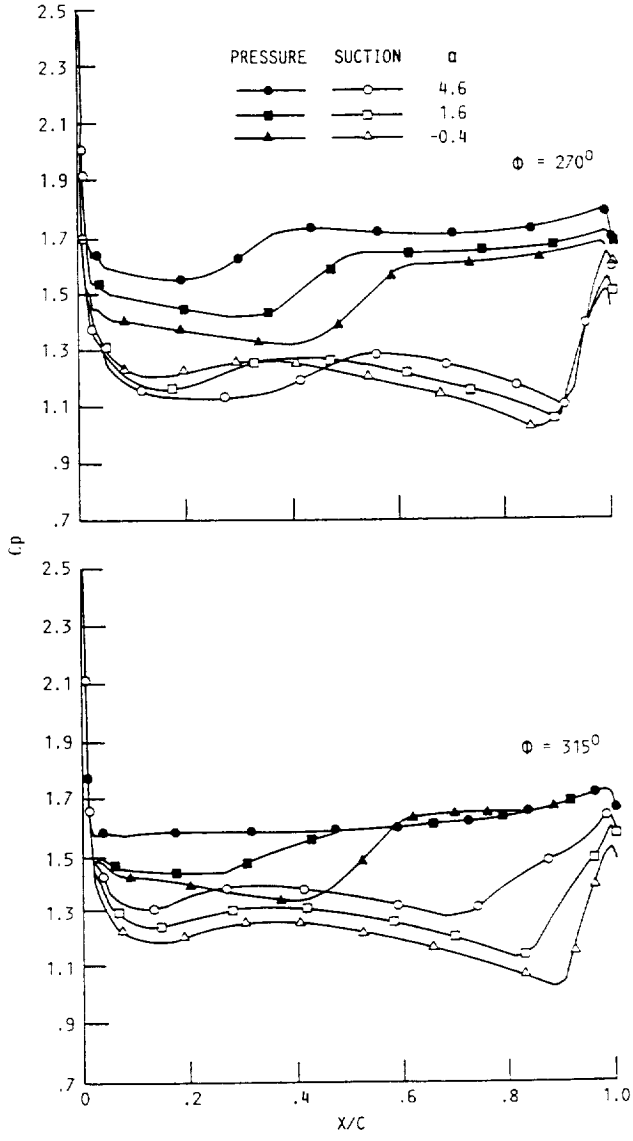

FIGURE 8. - CONCLUDED.

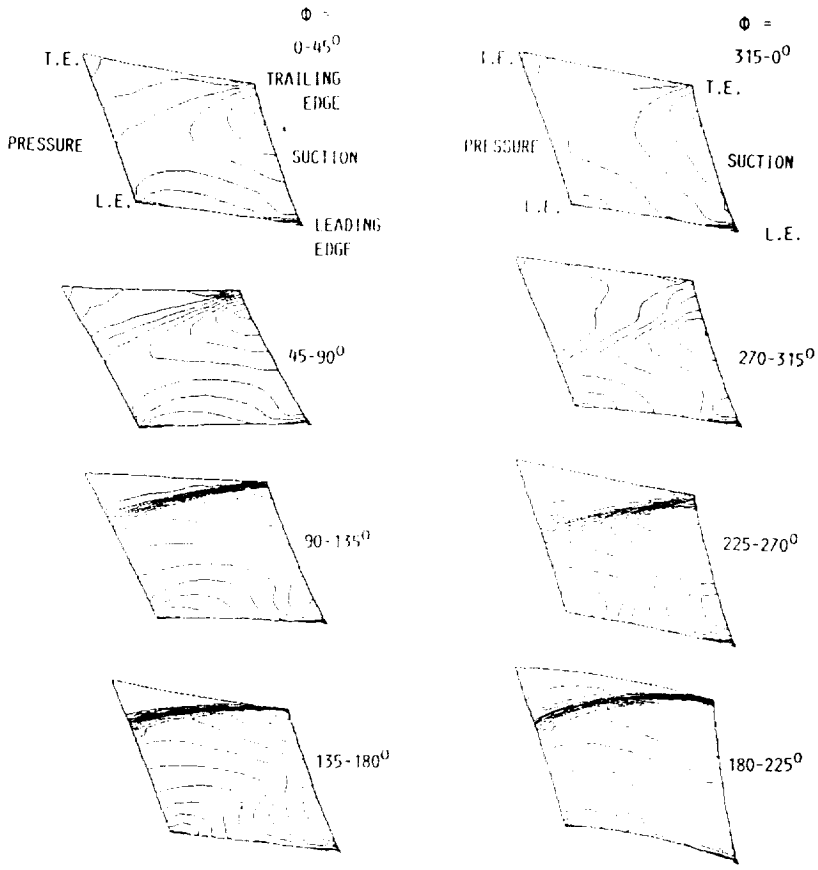

α = 4.6.

FIGURE 9. - PRESSURE CONTOURS IN THE BLADE PASSAGES AT r/R = 0.66, FOR AN INFLOW ANGLE OF 4.6 DEGREE (MIN = 0.15; MAX = 1.65; CONTOUR INTERVAL = 0.03).

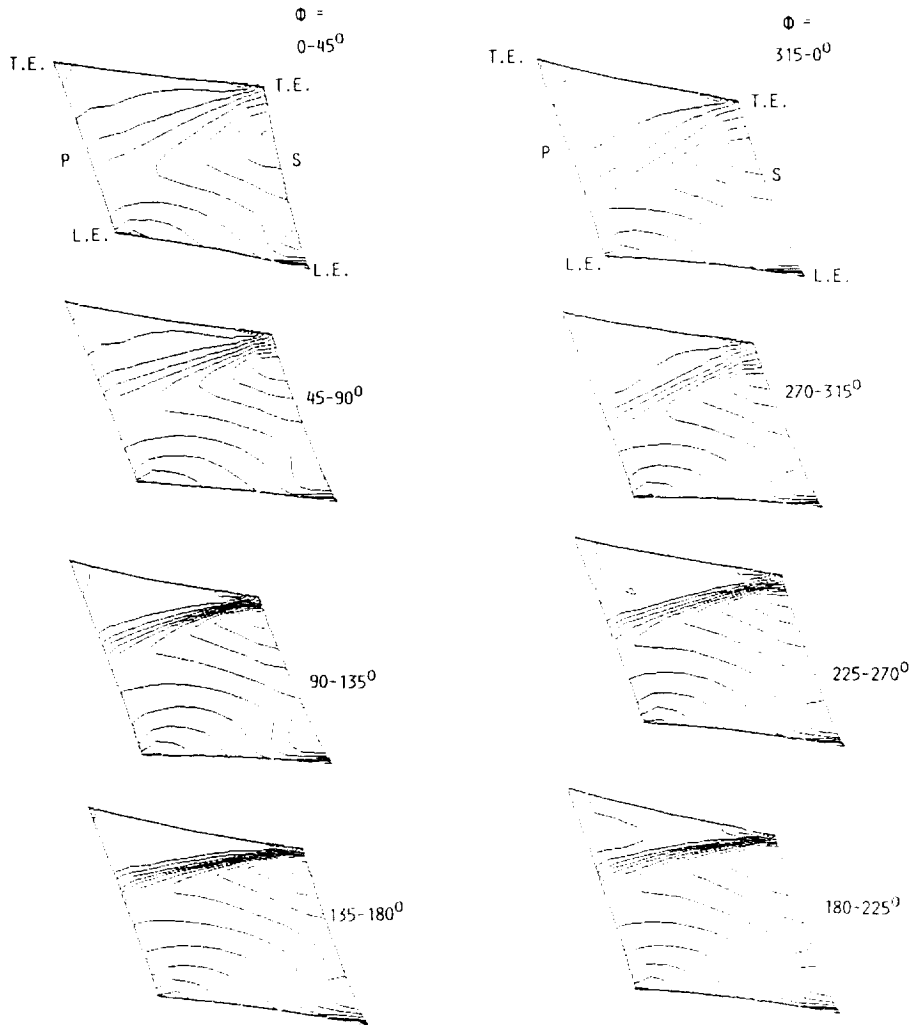

α = 1.6.

FIGURE 10. - PRESSURE CONTOURS IN THE BLADE PASSAGES AT r/R = 0.66, FOR AN INFLOW ANGLE OF 1.6 DEGREE (MIN = 0.15; MAX = 1.65; CONTOUR INTERVAL = 0.03).

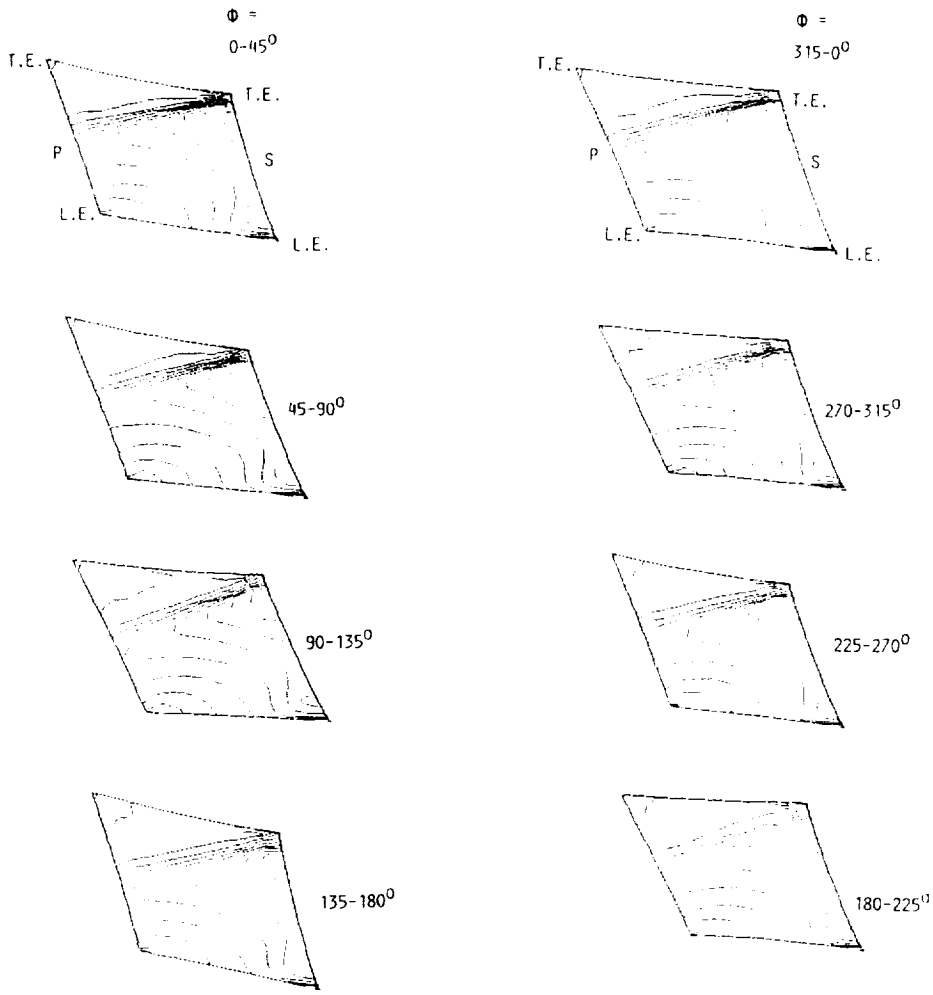

α = -0.4

FIGURE 11. - PRESSURE CONTOURS IN THE BLADE PASSAGES AT r/R = 0.66, FOR AN INFLOW ANGLE OF -0.4 DEGREE. (MIN = 0.15; MAX = 1.65; CONTOUR INTERVAL = 0.03).

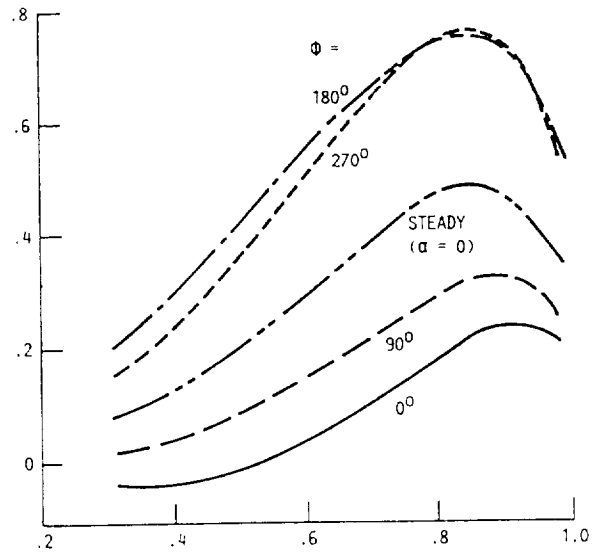

(a) α = 4.6.

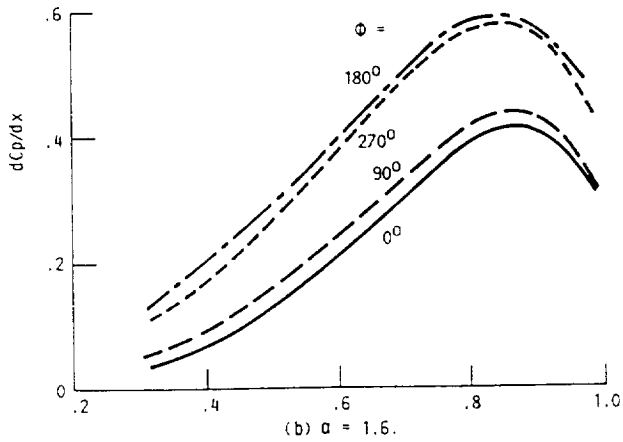

(b) α = 1.6.

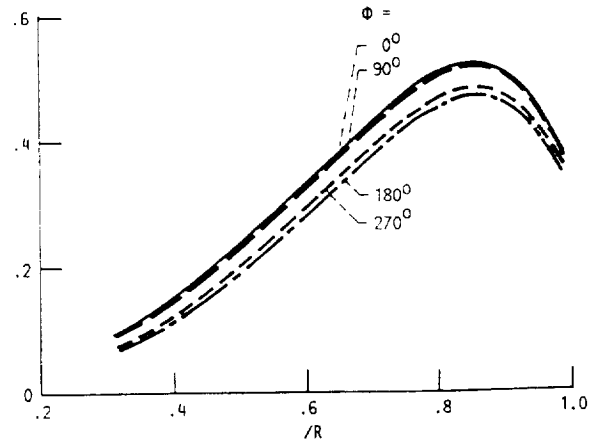

(c) α = -0.4.

FIGURE 12. - ELEMENTAL POWER COEFFICIENT VARIATIONS DURING A REVOLUTION.

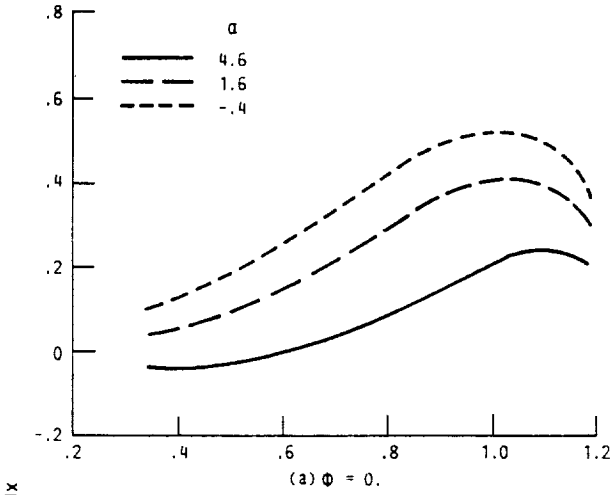

(a) Φ = 0.

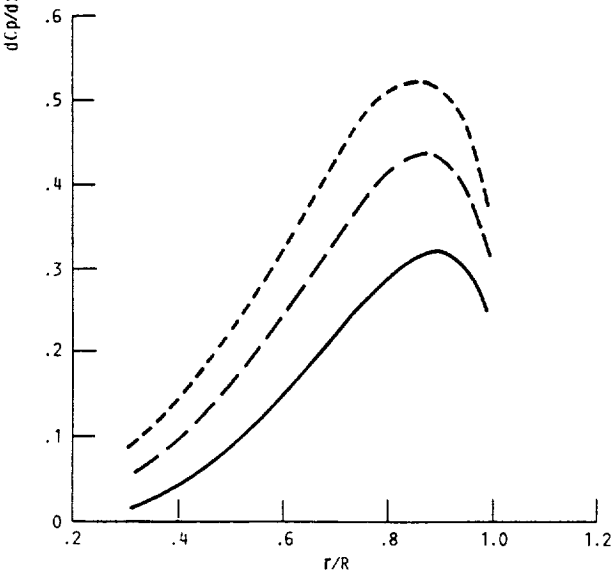

(b) Φ = 90.

FIGURE 13. - ELEMENTAL POWER COEFFICIENT VARIATIONS DUE TO INFLOW ANGLE.

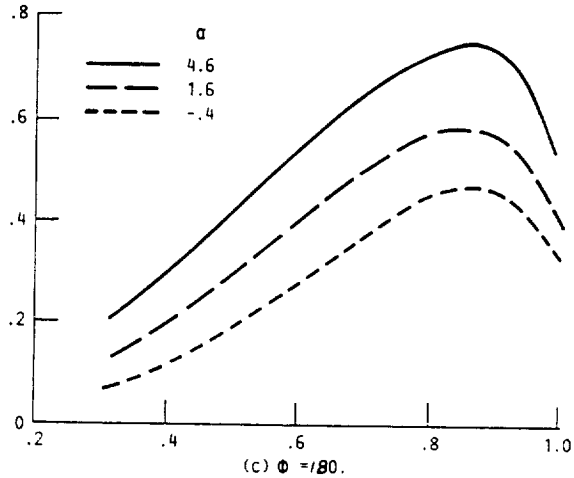

(c) Φ = 180.

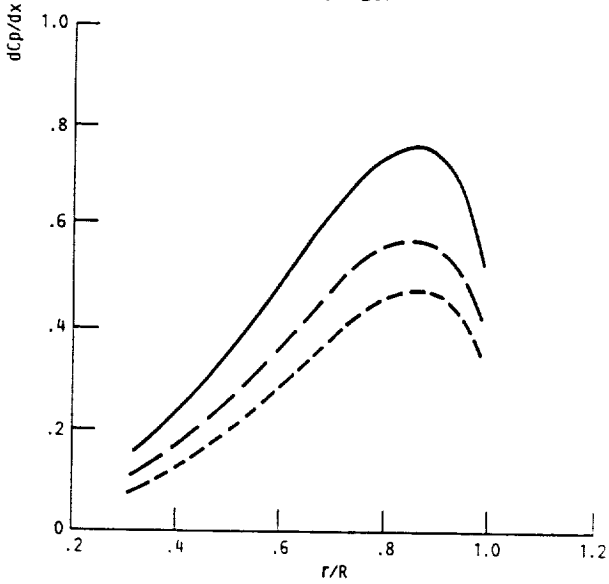

(d) Φ = 270.

FIGURE 13. - CONCLUDED.

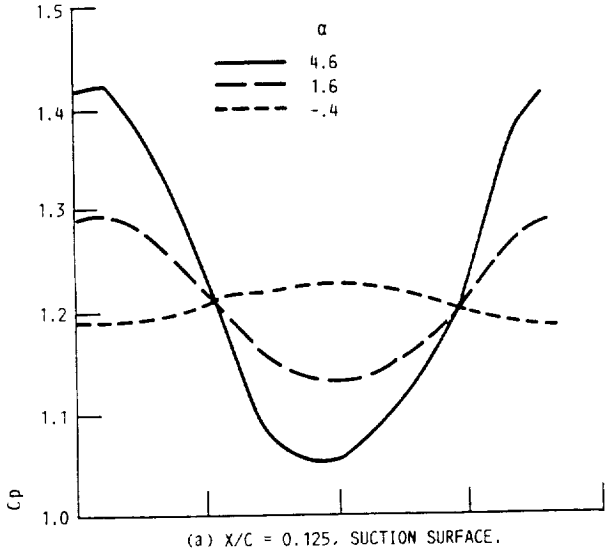

(a) X/C = 0.125, SUCTION SURFACE.

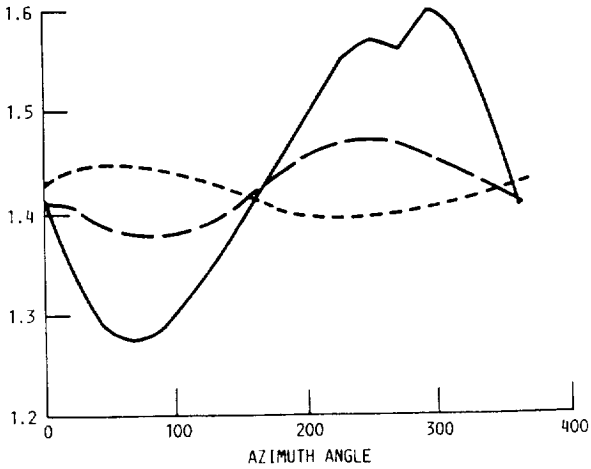

(b) X/C = 0.125, PRESSURE SURFACE.

FIGURE 14. - BLADE RESPONSE AT TWO DIFFERENT AXIAL LOCATIONS AT r/R = 0.66.

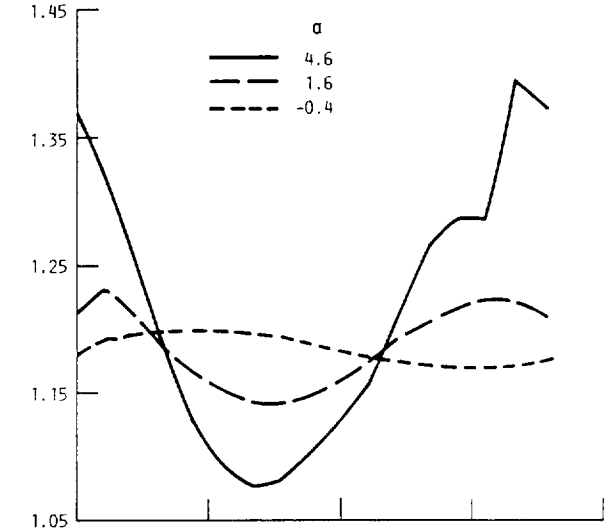

(c) X/C = 0.63, SUCTION SURFACE.

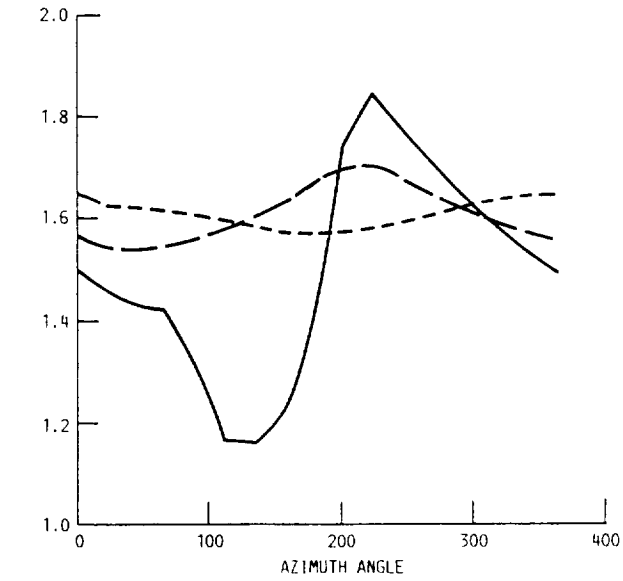

(d) X/C = 0.63, PRESSURE SURFACE.

FIGURE 14. - CONCLUDED.

NASA
National Aeronautics and Space Administration

Report Documentation Page

1. Report No.	2. Government Accession No.	3. Recipient's Catalog No.
NASA TM-102426 AIAA-90-0339		

4. Title and Subtitle	5. Report Date
Unsteady Euler Analysis of the Flow Field of a Propfan at an Angle of Attack	6. Performing Organization Code

7. Author(s)	8. Performing Organization Report No.
M. Nallasamy and J.F. Groeneweg	E-5191
	10. Work Unit No. 535-03-01

9. Performing Organization Name and Address	11. Contract or Grant No.
National Aeronautics and Space Administration Lewis Research Center Cleveland, Ohio 44135-3191	13. Type of Report and Period Covered Technical Memorandum

12. Sponsoring Agency Name and Address	14. Sponsoring Agency Code
National Aeronautics and Space Administration Washington, D.C. 20546-0001	

15. Supplementary Notes

Prepared for the 28th Aerospace Sciences Meeting sponsored by the American Institute of Aeronautics and Astronautics, Reno, Nevada, January 8-11, 1990. M. Nallasamy, Sverdrup Technology, Inc., NASA Lewis Research Center Group, Cleveland, Ohio 44135; J.F. Groeneweg, NASA Lewis Research Center.

16. Abstract

The paper examines the effects of angle of attack of a propfan on the blade loading and details of the flow field by solving the unsteady three-dimensional Euler equations. The configuration considered is the SR7L propeller at cruise condition and the inflow angles considered are 4.6°, 1.6° and −0.4°. The results indicate that the blade response is nearly sinusoidal at low inflow angles (1.6° and −0.4°) and significant deviations from sinusoidal behavior occur at an inflow angle of 4.6° due to the presence of strong shocks on both suction and pressure surfaces of the blade. The detailed flow in the blade passages shows that a shock formed on the suction surface during the highly loaded portion of the revolution extends across the passage to the pressure surface. An increase in inflow angle results in an increase in blade loading on the down-going side and a decrease in loading on the up-going side.

17. Key Words (Suggested by Author(s))	18. Distribution Statement
Advanced propellers Unsteady aerodynamics Three-dimensional Euler Analysis Angle of attack	Unclassified − Unlimited Subject Category 71

19. Security Classif. (of this report)	20. Security Classif. (of this page)	21. No. of pages	22. Price*
Unclassified	Unclassified	20	A03

NASA FORM 1626 OCT 86

*For sale by the National Technical Information Service, Springfield, Virginia 22161

National Aeronautics and
Space Administration

Lewis Research Center
Cleveland, Ohio 44135

FOURTH CLASS MAIL

ADDRESS CORRECTION REQUESTED

Official Business
Penalty for Private Use $300

Postage and Fees Paid
National Aeronautics and
Space Administration
NASA 451

NASA